

This work was written as part of one of the author's official duties as an Employee of the United States Government and is therefore a work of the United States Government. In accordance with 17 U.S.C. 105, no copyright protection is available for such works under U.S. Law.

Public Domain Mark 1.0

<https://creativecommons.org/publicdomain/mark/1.0/>

Access to this work was provided by the University of Maryland, Baltimore County (UMBC) ScholarWorks@UMBC digital repository on the Maryland Shared Open Access (MD-SOAR) platform.

Please provide feedback

Please support the ScholarWorks@UMBC repository by emailing scholarworks-group@umbc.edu and telling us what having access to this work means to you and why it's important to you. Thank you.



Short wavelength electromagnetic perturbations excited near the Solar Probe Plus spacecraft in the inner heliosphere: 2.5D hybrid modeling

Alexander S. Lipatov^{a,*}, Edward C. Sittler Jr.^b, Richard E. Hartle^b, John F. Cooper^b

^a Goddard Planetary Heliophysics Institute, UMBC/NASA GSFC, Code 673, Bld. 21, Rm. 247, 8800 Greenbelt Rd., Greenbelt, MD 20771, USA

^b NASA Goddard Space Flight Center, Greenbelt, MD 20771, USA

ARTICLE INFO

Article history:

Received 8 April 2011

Received in revised form

13 October 2011

Accepted 6 December 2011

Available online 14 December 2011

Keywords:

Solar wind

Spacecraft

Alfvén waves

Whistlers

Induced magnetospheres

Magnetic barrier

ABSTRACT

A 2.5D numerical plasma model of the interaction of the solar wind (SW) with the Solar Probe Plus spacecraft (SPPSC) is presented. These results should be interpreted as a basic plasma model derived from the SW interaction with the spacecraft (SC), which could have consequences for both plasma wave and electron plasma measurements on board the SC in the inner heliosphere. Compression waves and electric field jumps with amplitudes of about 1.5 V/m and (12–18) V/m were also observed. A strong polarization electric field was also observed in the wing of the plasma wake. However, 2.5D hybrid modeling did not show excitation of whistler/Alfvén waves in the upstream connected with the bi-directional current closure that was observed in short-time 3D modeling SPPSC and near a tether in the ionosphere. The observed strong electromagnetic perturbations may be a crucial point in the electromagnetic measurements planned for the future Solar Probe Plus (SPP) mission. The results of modeling electromagnetic field perturbations in the SW due to “shot” noise in absence of SPPSC are also discussed.

© 2011 Elsevier Ltd. All rights reserved.

1. Introduction

The study of the excitation of waves near a rapidly moving body has long history starting from the quasi-analytical approach (see e.g. Alpert et al., 1965; Alpert, 1974; and the references thereby) to recent electrostatic modeling (see e.g. Ergun et al., 2010; Olson et al., 2010). While the electrostatic studies produced very important information concerning charging of spacecraft, plasma void and wake, the problem of excitation of electromagnetic waves in the upstream and downstream flow near the spacecraft are of great interest to onboard measurements in the SW, magnetosphere and ionosphere. The electrostatic modeling, e.g., by Ergun et al. (2010) and Olson et al. (2010), based on stationary particle tracing and computing the electrostatic potential do not include the non-stationary phenomena and a gap between heat shield and bus of the SC. Note that 3D electrostatic modeling with stationary tracing of electrons and cold protons was recently performed by Ergun et al. (2010) in case of very small Debye length, $\lambda_D \ll L$ whereas modeling of the Cassini spacecraft by Olson et al. (2010) does not resolve the Debye length. Numerical modeling of the interaction of space plasma

with a SC plays a key-role in understanding how electromagnetic perturbations may effect the scientific measurements on board the SC. This is especially true for SPP where new regimes of SW are being explored. Modeling provides the general characteristics of the plasma environment and the electromagnetic field distribution near the probe and at its surface. The external surface of the SPPSC consists of a conducting part and an insulating part. It moves in supersonic/subsonic and superalfvénic/subalfvénic SW flow.

Numerical modeling of the interaction of space plasma with spacecraft devices plays a key-role in their design. This is especially true for SPP where new regimes of solar wind plasma are being explored. Modeling provides general characteristics of the plasma environment and the electromagnetic field distribution near the probe and at its surface. The external surface of the SPP consists of a conducting part and an insulating part. It moves in the supersonic/subsonic and superalfvénic/subalfvénic solar wind flow.

A first approximation to the plasma environment near the SPP may be similar to the plasma environment near the Moon with a weakly conducting surface. In the case of a non-conducting model of the Moon, solar wind particles penetrate the surface on the day-side of the Moon, whereas on the night-side a plasma wake with a low-density void is formed. On the day side of the Moon's surface, plasma particles are absorbed, and a perturbation region forms a thin boundary layer of thickness

* Corresponding author. Tel.: +1 301 286 0906; fax: +1 301 286 1648.

E-mail addresses: Alexander.Lipatov-1@nasa.gov, alipatov@umbc.edu (A.S. Lipatov).

$\delta \sim c/\omega_{pe} \propto 1 \text{ km}$ at 1 AU. (Neugebauer, 1960). On the night side the perturbation region is bounded by a surface of weak perturbations forming a cone with half-apex angle $\sin^2 \theta = 1/M_A^2 + 1/M_S^2$ ($M_A \propto 8$ and $M_S \propto 8$ are the Alfvén and sound Mach numbers, $V_A \approx 50 \text{ km/s}$, $w_{th} \approx 50 \text{ km/s}$, $U \approx 400 \text{ km/s}$, and $\theta \approx 10^\circ$) (Wang, 1969; Lipatov, 1976).

No bow shock or oblique Mach cone are formed. Perturbation of the magnetic field inside the plasma wake is mostly determined by a diamagnetic current and drift currents due to a curvature of the magnetic field and acceleration of the bulk velocity (Wang, 1968, 1969; Wang and Ness, 1970; Lipatov, 1976, Lipatov, 2002). Kinetic instabilities may also play a role in wake dynamics. Hybrid modeling of the interaction between supersonic plasma flow and a weakly conducting body shows formation of a strong oblique double shock structure inside the plasma wake (Lipatov et al., 2005).

The goal of our research is the study of several aspects of the interaction of the solar wind with the SC when $r = 9.5 R_S$: (a) plasma wake formation, (b) a quasi-stationary electric and magnetic field configuration, (c) excitation of the electromagnetic field perturbations resulting from upstream and downstream SW flow at the spacecraft. The 2.5D modeling was used for task (a) including a study of the formation of a strong polarization electric field in the wings of the plasma wake. The 3D hybrid modeling was used for tasks (b) and (c) including the study of the excitation of the electromagnetic perturbations and a formation of the bi-directional current system in upstream and downstream flow near the SC. In this article we only discuss the 2.5D hybrid modeling results. Even short time 3D hybrid modeling ($0.1 T_{transit}$) needs 5 months of computing with 24 cores in the OpenMP environment. We expect to produce long time 3D modeling in a hybrid MPI/OpenMP environment with thousands of a core computing. The results of such modeling will be discussed in future publications.

The paper is organized as follows: in Section 2 we present the computational model and a formulation of the problem. In Section 3 we present the results of the 2.5D hybrid modeling of the plasma environment near the SPPSC. Finally, in Section 4 we summarize our results and discuss the future development of our computational model.

2. Formulation of the problem and mathematical model

2.1. Solar wind model

The interaction of the solar wind with the SPP is more complicated because the gyroradius of the protons (for Maxwellian core of the velocity distribution 1–500 km) is much larger than the size of the spacecraft (2–3 m). For energetic components the ion gyroradius may be extremely large with respect to the spacecraft. So the kinetic approximation for ions is an essential part of the mathematical model. The electron gyroradius may vary in range from $2.5 \times 10^2 \text{ m}$ at Earth orbit to much smaller scale, 1 m, near Sun. Therefore, electrons need a fluid-kinetic approximation to study the plasma environment along the SPP trajectory.

The present model of the interaction of the solar wind with the SPP does not take into account several effects of the plasma environment near the spacecraft. Future modeling will take into account charging of the spacecraft, charge separation, outgassing from the heat shield, photoionization and electron impact ionization near the spacecraft. Our modeling will serve as an expert system for design of the SPPSC.

To study the interaction of the solar wind with the SPPSC we use a quasi-neutral hybrid model for ions and electrons.

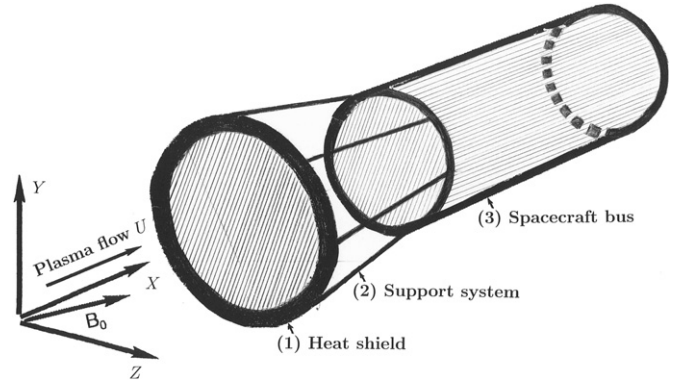


Fig. 1. Scheme of the interaction of the solar wind with SPP. The spiral magnetic field is inside the x - z plane: (1) a heat shield, (2) a support system, and (3) a spacecraft bus.

In our coordinate system the X (radial) axis is parallel to the solar wind velocity— \mathbf{U}_0 , Z is aligned with the equatorial plane, and $\mathbf{Y} = \mathbf{Z} \times \mathbf{X}$, Fig. 1.

In the hybrid modeling described here, the dynamics of upstream ions is described by a kinetic approach, while the dynamics of the electrons is described by a hydrodynamical approximation.

The single particle ion distribution function $f_i(t, \mathbf{x}, \mathbf{v})$ has to satisfy the Vlasov/Boltzmann equation

$$\frac{\partial}{\partial t} f_i + \mathbf{v} \cdot \frac{\partial}{\partial \mathbf{x}} f_i + \frac{\mathbf{F}}{M_i} \cdot \frac{\partial}{\partial \mathbf{v}} f_i = F_{coll}, \quad (1)$$

where \mathbf{F} symbolizes forces due to electric and magnetic fields acting on the ions, F_{coll} is the collision term. In this paper we use the particle-mesh model for ion dynamics instead of the Vlasov equation, Eq. (1).

The single ion particle motion is described by the equations (see e.g., Mankofsky et al., 1987, Eqs. (1) and (14)):

$$\frac{d\mathbf{r}_{i,l}}{dt} = \mathbf{v}_{i,l}, \quad \frac{d\mathbf{v}_{i,l}}{dt} = \frac{e}{M_i} \left(\mathbf{E} + \frac{\mathbf{v}_{i,l} \times \mathbf{B}}{c} \right) - \frac{m_e v_{ie}}{M_i e n_i} \mathbf{J}. \quad (2)$$

Here we assume that the charge state is $Z_i=1$ and that all ions have the same mass M_i . \mathbf{U}_i and \mathbf{J} denote the charge-averaged velocity of all (incoming and pickup) ions and the total current, Eq. (6). The subscript i denotes the ion population and the index l is the macro-particle index. v_{ie} is collision frequency between ions and electrons, that may include Coulomb collisions and collisions due to particle-wave interaction. Note that the collision rates used in Eq. (2) must depend on the individual velocities of ions and electrons. However, we use the effective resistivity η , $\eta = \sigma^{-1} = m_e / (ne^2 \tau_e)$, where $\tau_e = v_{ie}^{-1}$. The electrical conductivities may be estimated as

$$\sigma_{\perp} = \sigma_1 T_e^{3/2}, \quad \sigma_{\parallel} = 1.92 \sigma_{\perp}, \quad \sigma_1 = 0.9 \times 10^{13} / ((A/10) Z_i) s^{-1} \text{ eV}^{-3/2}, \quad (3)$$

where T_e denotes the electron temperature and A is the Coulomb logarithm (see e.g., Braginskii, 1965, pp. 215–216). For typical solar wind parameters at a distance, $r = 9.5 R_S$, $T_e = 100 \text{ eV}$ (electron temperature), $n_0 = 5 \times 10^3 \text{ cm}^{-3}$ (density), and electrical conductivities are $\sigma_{\perp} \approx 4.7 \times 10^{13} \text{ s}^{-1}$ and $\sigma_{\parallel} \approx 9.2 \times 10^{13} \text{ s}^{-1}$.

In our modeling we use the value of the effective conductivity that is much smaller than the real value to suppress “shot” noise. The numerical “shot” noise is a result of a fluctuation in density and bulk velocity due to the small number of particles per cell in the particle in cell modeling. We also use an effective conductivity for modeling SPP’s bus. Hence, we must keep the first collision term in the right hand side of Eq. (2).

In the non-radiative limit Ampère's law is given by

$$\frac{4\pi}{c}\mathbf{J} = \nabla \times \mathbf{B} \quad (4)$$

and the induction equation (Faraday's law) by

$$\frac{1}{c}\frac{\partial \mathbf{B}}{\partial t} + \nabla \times \mathbf{E} = 0. \quad (5)$$

The total current is given by

$$\mathbf{J} = \mathbf{J}_e + \mathbf{J}_i, \quad \mathbf{J}_i = en_i \mathbf{U}_i. \quad (6)$$

We further assume quasi-neutrality

$$n_e \approx n_i. \quad (7)$$

The equation of motion of the electron fluid takes the form of the standard generalized Ohm's law (e.g., Braginskii, 1965):

$$\mathbf{E} = \frac{1}{en_e c}(\mathbf{J}_e \times \mathbf{B}) - \frac{1}{en_e} \nabla p_e + \frac{m_e}{e} \mathbf{v}_{e,i} \frac{\mathbf{J}}{ne} - \frac{m}{e} \frac{d}{dt} \mathbf{U}_e, \quad (8)$$

where $p_e = nm_e \langle v_e^2 \rangle / 3 = n_e k_B T_e$, and v_e' are the scalar electron pressure and the thermal velocity of electrons, $v_e' = 5000$ km/s, and the electron current is estimated from Eq. (6). The last term on the right side of Eq. (8) is the electron inertial term.

Since we suppose that electron heating due to collisions with ions is very small, the electrons are considered as an adiabatic fluid. For simplicity we assume that the electron pressure may be represented as

$$p_e \propto n_i^{5/3}. \quad (9)$$

We also assume that $n_e \approx n_i$. Otherwise, we have to calculate the electron pressure from the heat balance for electrons (see e.g., Braginskii, 1965) taking into account the heat fluxes. The hybrid model allows us to study the dynamics of the ion velocity distribution and the effects of a finite ion gyroradius. The electron gyroradius and charge separation effects are not resolved in hybrid models, therefore we have to use a full kinetic model in future modeling.

2.2. SPP spacecraft model

Fig. 1 shows a scheme of the SPPSC, a system of coordinates and the directions of plasma flow and magnetic field. The SPP model includes three main parts, namely, a non-conducting heat shield (1), a support system (2), and a cylindrical section or spacecraft bus (3) that contains the particle analysis devices and antenna. The heat shield has the following geometrical parameters: diameter, $D_{\text{shield}} = 2.7$ m, and thickness = 0.335 m. The gap between the heat shield and cylindrical section is 1.188 m. Note the gap is now covered with radiators, so there is no penetration of the solar wind through the radiators. The cylindrical section or bus has a diameter of 1.026 m and length 1.188 m. We also take into account the effective resistivity of the SPP's bus, the heat shield and the gap between the heat shield and the spacecraft bus:

$$\begin{aligned} \rho_{\text{bus}} &= 1.2 \times 10^{-3} \Omega \text{ m}, \\ \rho_{\text{shield}} &= 6 \Omega \text{ m}, \quad \rho_{\text{gap}} = 1.2 \Omega \text{ m}. \end{aligned} \quad (10)$$

Our code solves Eqs. (1)–(9). Here we note that the gap has several trusses to provide a mechanical interface between bus and heat shield. If electrical conductivity of the trusses is high enough so that differential charging between spacecraft bus and heat shield is low, then the heat conduction from heat shield to spacecraft bus may be too high. At this time we still do not know the exact values of the truss electrical conductivity parameters.

Initially the computational domain contains only supersonic or subsonic solar wind flow with a homogeneous spatial distribution. The magnetic field and electric fields are $\mathbf{B} = \mathbf{B}_0$ and

$\mathbf{E} = \mathbf{E}_0 = -\mathbf{U}_0 \times \mathbf{B}_0$. Inside the Solar Probe spacecraft the electromagnetic fields are $\mathbf{E} = 0$ and $\mathbf{B} = \mathbf{B}_0$, and bulk velocities of ions and electrons are also equal to zero. In the cases examined here we choose a spiral angle $\theta_{bu} = 11^\circ$ for the magnetic field.

Far upstream ($x = -DX/2$), the ion flux is assumed to have a Maxwellian distribution,

$$f = n_\infty (\pi v_{th}^2)^{-3/2} \exp \left[-\frac{(\mathbf{v} - \mathbf{U})^2}{2v_{th}^2} \right], \quad (11)$$

where v_{th} and \mathbf{U} are the thermal and the bulk velocities of the solar wind plasma flow. We have not included a contribution from the field aligned Strahl electrons which are non-Maxwellian.

Far downstream, we use a buffer zone to provide the return of particles with negative values of the u velocity component. We also adopted Sommerfeld's radiation condition for the magnetic field. On the side boundaries ($y = \pm DY/2$), unperturbed boundary conditions were imposed for the incoming flow particles and the electromagnetic field. To prevent the reflection of the waves on the boundaries we used a strong dissipation of waves ($l_{eff,d} = 1/Re_{eff,m} = 160$) in the outer region, $r > 6L$. At the spacecraft surface the particles are absorbed. There is no boundary condition for electromagnetic fields. We use our equations for the electromagnetic fields inside the spacecraft with internal conductivity and bulk velocity calculated from the particles. In this way the jump in the electric field is due to the variation of the values of conductivity and bulk velocity across the surface of the SPPSC. The position of the center of the bottom of the heat shield is defined as $x = 0, y = 0$.

The 2D computational domain has dimensions $DX = 24L$, and $DY = 16L$ (or $DX = 10L$, and $DY = 8L$), where $L = D_{\text{shield}}/2 = 1.35$ m is the radius of the heat shield. We use a mesh of 601×401 grid points for the results discussed here, and 9×10^8 particles for protons in a homogeneous mesh computation. We use a subcycling procedure for time integration of the particle and the electromagnetic equations (see e.g., Lipatov, 2002). The time step for the particle update, Δt_p , satisfies the condition $v_{\text{max}} \Delta t_p \leq \min(\Delta x, \Delta y)/16$, whereas the time step for the electromagnetic field time integration, Δt_f , is much smaller than the time step for particle update. Δt_f satisfies the condition $v_{\text{max}} \Delta t_f \leq \min(\Delta x, \Delta y)/(12800 \times 16)$. The grid spacings are as follows: $\Delta x = \Delta y = 0.054$ m.

The relationships between dimensional ($\mathbf{U}, \mathbf{E}, \mathbf{B}, p_e, n, T$) and dimensionless ($\mathbf{U}', \mathbf{E}', \mathbf{B}', p_e', n', T'$) parameters may be expressed via the dimensional upstream values as follows:

$$\mathbf{U} = \mathbf{U}' U_0, \quad \mathbf{E} = \mathbf{E}' B_0 U_0 / c, \quad \mathbf{B} = \mathbf{B}' B_0, \quad p_e = p_e' p_{e0},$$

$$n = n' n_0, \quad T = T' M_i U_0^2, \quad (12)$$

whereas the dimensional time and distance may be expressed via the bulk velocity U_0 and characteristic scale $L = D_{\text{shield}}/2$:

$$t = t' L / U_0, \quad x = x' L. \quad (13)$$

Note that we shall use the dimensionless parameters for a presentation of the results of modeling in Section 3.

The global physics in SPP's environment is controlled by a set of dimensionless independent parameters such as Alfvén Mach number M_A , ion and electron plasma betas $\beta_i = p_i / (4\pi B_0^2)$, $\beta_e = p_e / (4\pi B_0^2)$, electron/proton mass ratio m/M_p , diffusion lengths, and the gyroradius $\epsilon = \varrho_{ci} / L$. Here $\varrho_{ci} = U_0 / (eB / M_i c) = M_A c / \omega_{pi}$ and the ion plasma frequency $\omega_{pi} = \sqrt{4\pi n_0 e^2 / M_i}$. The actual value of the proton gyroradius is about 0.31–2.5 km using the above formulas. The grid spacing has the value $\Delta x = (0.02–0.04)L = (0.036–0.072)$ m, so that the ion gyroradius is resolved on the grid.

2.3. Numerical implementation

We employed a standard particle-in-cell (PIC) method with a homogeneous grid. The time integration of the particle equations of motion uses a trapezoidal leapfrog scheme (see e.g., Lipatov, 2002). The time integration of the electromagnetic field equations uses an implicit finite difference scheme (see e.g., Lipatov, 2002).

One 2.5D hybrid modeling takes around one month for computing with 24 processors and 64 GB RAM on the “shared memory” Columbia SGI system at the NASA Advanced Supercomputing (NAS) Division, Ames Research Center. Currently, our code operates in the parallel processing with the OpenMP environment. Converting the 3D and 2.5D codes to the hybrid MPI/OpenMP environment was performed by technical staff members of the Software Integration and Visualization Office (NASA GSFC) starting from Spring 2008 and we have now tested the hybrid MPI/OpenMP and OpenMP versions of the code on Pleiades and Discover massively parallel supercomputers with distributed memory.

3. Results of the modeling

To study the interaction of solar wind with the SPP we use the following sets of solar wind plasma parameters: $\beta_i = 0.1$ ($T_i = 1\text{MK}$); $\beta_e = 0.1$ ($T_e = 1\text{MK}$); magnetic field, $B_0 = 1500\text{ nT}$; bulk velocity $U_0 = 200\text{ km/s}$, density $n_{SW} = 5 \times 10^3\text{ cm}^{-3}$, Alfvén Mach number $M_A = 1–1.5$ and $\theta_{bu} = 0–11^\circ$ (see Table 1 and Murphy et al., 2008). The value of the plasma bulk velocity in the spacecraft frame may vary from 200 km/s to 800 km/s so we can use a higher Alfvén and sonic Mach numbers in our modeling. To exclude the statistical fluctuation for larger ion velocities we cut the wing of the Maxwellian velocity distribution at $v = 5V_{th}$. Table 2 shows all parameters that correspond to our case. These parameters correspond to the values of the motional electric field $E_0 \approx 0.3\text{ V/m}$ for $r = 9.5R_S$. We present the results of modeling at the distance, $r = 9.5R_S$. In the present modeling, the dimensionless scale of the proton gyroradius is $\epsilon = \rho_p/L = 10^3$.

Since 3D hybrid modeling of the SPPSC’s environment is very costly we have also performed a set of 2.5D models. The results of the 3D hybrid modeling will be discussed in a future publication. The 2.5D modeling includes both the particle absorption boundary condition at the heat shield and the particle absorption boundary condition on the heat shield (the later case is not discussed here). The 2.5D hybrid modeling of the oblique and quasi-parallel interaction shows the unphysical growth of the magnetic field barrier since the magnetic field line cannot penetrate though the cylindrical obstacle. Here we present only the cases with a parallel interaction, $\theta = 0^\circ$. We use 880×10^6

macro-particles and a mesh with 401×601 grid points so that we have 3675 particles per cell in our 2.5D modeling. The thermal velocity distribution for macro-particles is generated in the velocity interval $\Delta v = \pm 5v_{i,th}$.

3.1. Perturbations in the presence of the SPP spacecraft

Let us consider now the results of the modeling with $\beta_e = 0.1$ at time, $t = 15 T_{ce}$ ($t = 20 T_{transit}$), where $T_{transit}$ is the time for particle transit from the left boundary to the right boundary of the computational domain. Fig. 2 shows a global distribution of the proton density and the electromagnetic field components in the $y-x$ plane. We see the formation of the large void behind the heat shield and the bus.

Fig. 2(b), (c) and (d) shows distributions for the electric field at $t = 15 T_{ce}$. As before, the perturbations in the electromagnetic field reached saturation levels.

The electric field upstream is calculated by the use of the simplified generalized Ohm’s law in dimensionless form:

$$\mathbf{E} = -\mathbf{U}_i \times \mathbf{B} + \frac{\epsilon}{M_A^2 n_e} ((\nabla \times \mathbf{B}) \times \mathbf{B}) - \frac{\epsilon \beta_e}{2 M_A^2 n_e} \nabla p_e. \quad (14)$$

At a distance $r = 9.5R_S$ the typical values of the gyroradius $\epsilon = \rho_{ci}/L$, M_A and β_e are 10^3 , 0.1 and 1.5 so that any small perturbation in the magnetic field or density results in an excitation of a very strong perturbation in the electric field. This fact may distinguish the physics of the solar wind interaction with a small objects from a standard interaction of the plasma flow with planets and moons, where this parameter is a smaller or about the unity. Since the modeling does not show any perturbations in bulk velocity upstream we can conclude that the perturbations in the electric field E_y and E_z are whistler-like and these perturbations with $E_y \neq E_z$ are due to the second term in the right side of Eq. (14) (Hall term).

Figs. 3 and 4 show 1D cuts for the electric field profile along the x and y axes through the point $y=0$ and $x=1.5$, respectively.

Far from the spacecraft, the values of perturbation in the electric field components, E_x , E_y and E_z are about of $\delta E_x \approx \delta E_y \approx \pm 2.0 E_0$ and $\delta E_z \approx 0.1 E_0$ in the x -direction (upstream and downstream). The values of perturbation in the electric field components, E_x , E_y and E_z , are about of $\delta E_x \approx \delta E_y \approx \pm (1.0–2.0)E_0$ (oblique whistler/Alfvén waves or “shot noise”) in the y -direction, and $\delta E_z \approx 0.02E_0$ in the y -direction.

Near the spacecraft, the E_x profile has a jump, $\delta E_x \approx (+14.0, -33.0)E_0$ in the x -direction behind the heat shield and the bus, respectively. We also see a jump in E_y component of the electric field, $\delta E_y \approx (+15.0, -38.0)E_0$ in x -direction behind the bus and $\delta E_y \approx \pm 55.0E_0$ in y -direction, also near bottom of bus. The component E_z has jumps, $\delta E_z \approx (-0.4, 0.3)E_0$ in the x -direction, and $\delta E_z \approx -(0.4, 0.05)E_0$ in the y -direction, Figs. 3 and 4, respectively.

Let us consider the structure of the plasma wake in detail. Fig. 2 shows the formation of wing-like structures in the electric field profiles. The main part of the perturbations in the electric field inside the wing are due to a strong gradient in the density in x and y directions, $E_x = 7E_0$ and $E_y = 50E_0$. Fig. 2(d) shows excitation of the electric field component, E_z , both upstream and downstream. Along the x -axis the perturbations are $E_z = 0.06E_0$ upstream and $E_z = 0.02E_0$ downstream are shown in Fig. 3(d).

Table 1
Important values of the electromagnetic field in an antenna (Murphy et al., 2008).

Parameters	$4R_S$	$12R_S$	$20R_S$
$U \times B$	12 V/m	2.5 V/m	0.5 V/m
$E_{max, DC}$	1 V/m	0.1 V/m	0.1 V/m
$E_{max, 100\text{ kHz}}$	$10^{-3}\text{ V/m Hz}^{-1/4}$	$10^{-4}\text{ V/m Hz}^{-1/4}$	$10^{-4}\text{ V/m Hz}^{-1/4}$
V Noise at 100 kHz	$10^{-6}\text{ V/Hz}^{-1/4}$	$3 \times 10^{-7}\text{ V/Hz}^{-1/4}$	$2 \times 10^{-7}\text{ V/Hz}^{-1/4}$

Table 2
Solar wind parameters for modeling.

Case	U_0	n_{SW}	B_0	θ_{bu}	M_A	β_p	β_e	$U_0 \times B_0$	N_p per cell	Comments
a	200 km/s	5×10^3	1500 nT	0°	1.5	0.1	0.1	0.3 V/m	800	2.5D, with absorption
b	200 km/s	5×10^3	1500 nT	0°	1.5	0.1	0.1	0.3 V/m	800	2.5D, with absorption; higher spatial resolution

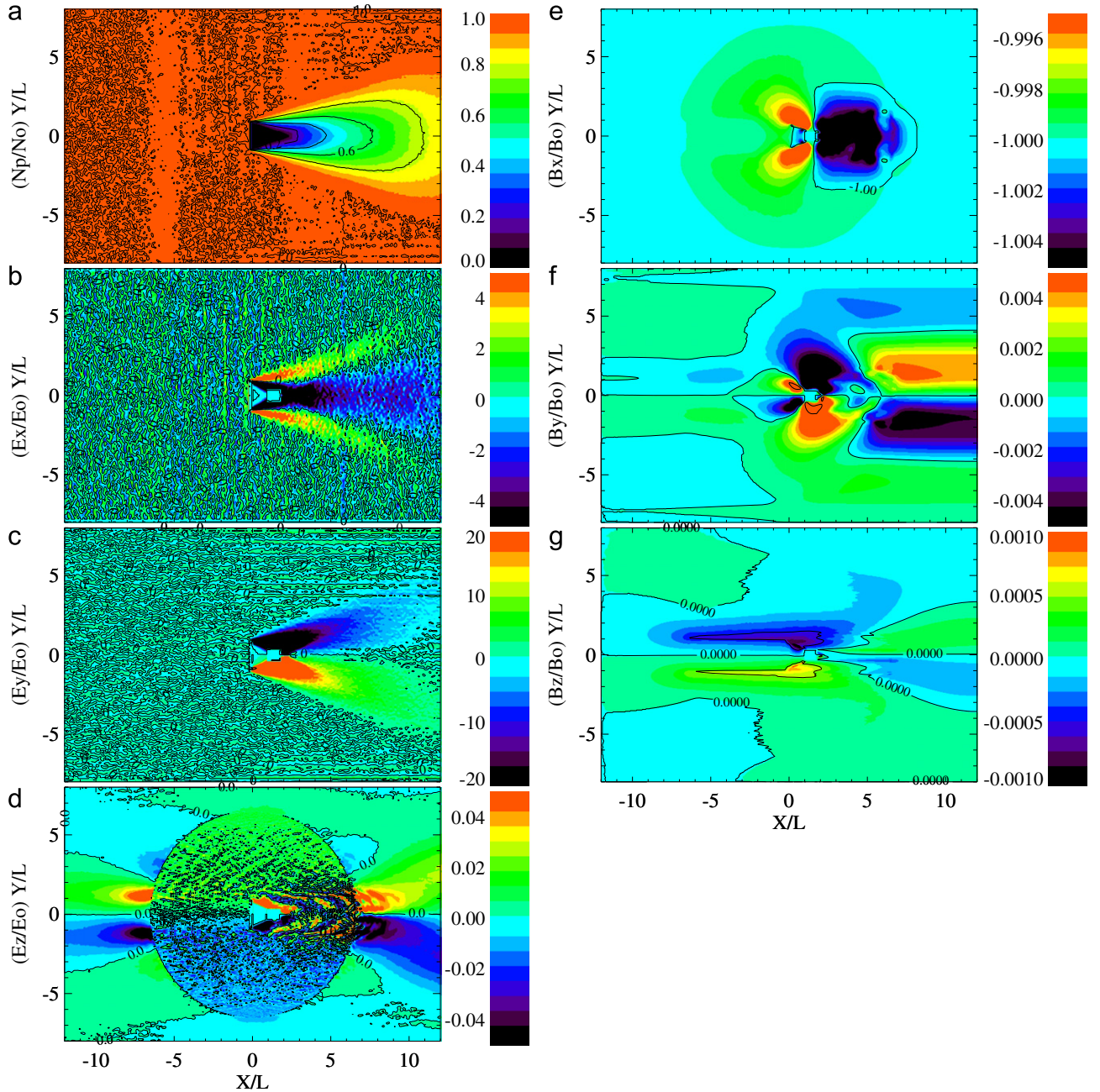


Fig. 2. Solar wind ion density (a), the electric (b,c,d) and magnetic (e, f, g) fields in the y - x plane. $E_0 = U_0 B_0 = 0.3$ V/m, $N_0 = 5 \times 10^3$ cm $^{-3}$, $\theta_{bu} = 0^\circ$. Non-linear saturation of the perturbations at $t = 15T_{ce}(20T_{transit})$.

The wavelength is about $\lambda = L/2 = 0.675$ m. Figs. 2(d), 3(e) and (f) show much stronger perturbations in the E_z at the distance $y = \pm L$ from the center line ($y=0$). Inside the region with $r < 6L$, perturbations in the E_z component are $(0.1-0.2)E_0$ and the wavelength is about $\lambda \propto L \propto 1$ m. In outer region with $r > 6L$ the damping is very strong and we see only long wavelength perturbations as shown in Fig. 2(d).

The above figures demonstrate a strong oscillation in the electric field. The fluctuation in the polarization electric field due to “shot” noise (in plasma density) may be estimated as

$$\delta E_{pol} \approx -\frac{\epsilon \beta_e}{2M_A^2 n_e} \nabla p'_e. \quad (15)$$

Since, a fluctuation in the density due to “shot” noise is about, $(\delta n)/n = 1/\sqrt{N_p}$ (see e.g., Birdsall et al., 1970) we can express the

fluctuation in the electric field as the following:

$$\delta E_{pol} \approx -\frac{\epsilon \beta_e}{2M_A^2 \Delta x \sqrt{N_p}}, \quad (16)$$

where Δx is a grid spacing.

If we assume the “shot” noise $(\delta n)/n = 0.016$ then a $\delta E_{pol} \approx 25 E_0$. This value represents the upper limit for the polarization electric field.

Fig. 2(e), (f) and (g) demonstrates distributions for the magnetic field. At the front of the heat shield, formation of a magnetic field barrier or build up was observed. At the side parts of the computational domain, compression waves were observed while modeling. The value of the perturbation in the magnetic field is about $\delta B \approx 0.02 B_0$.

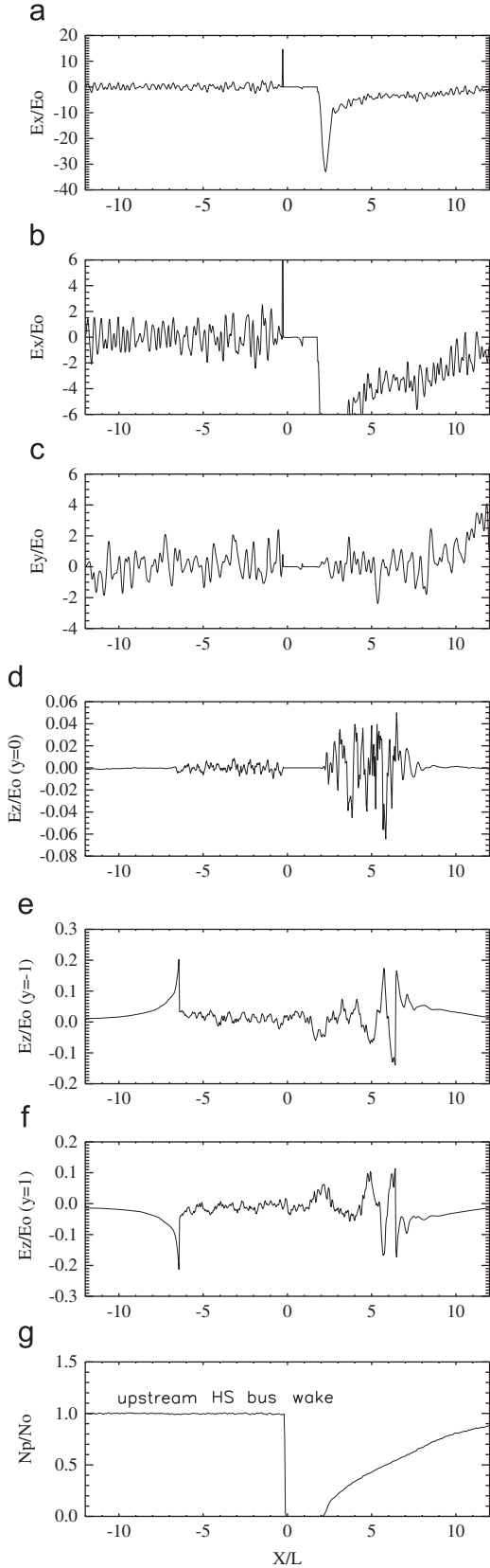


Fig. 3. The 1D cuts for the electric field components $E_x(E_0)$, $E_y(E_0)$ and $E_z(E_0)$ ($y=0$). Non-linear saturation of the perturbations at $t = 15 T_{ce}$.

Table 3 accumulates the results of the modeling presented in this paper. Here we show the level of fluctuations in the electric field produced in regular modeling and in modeling with the

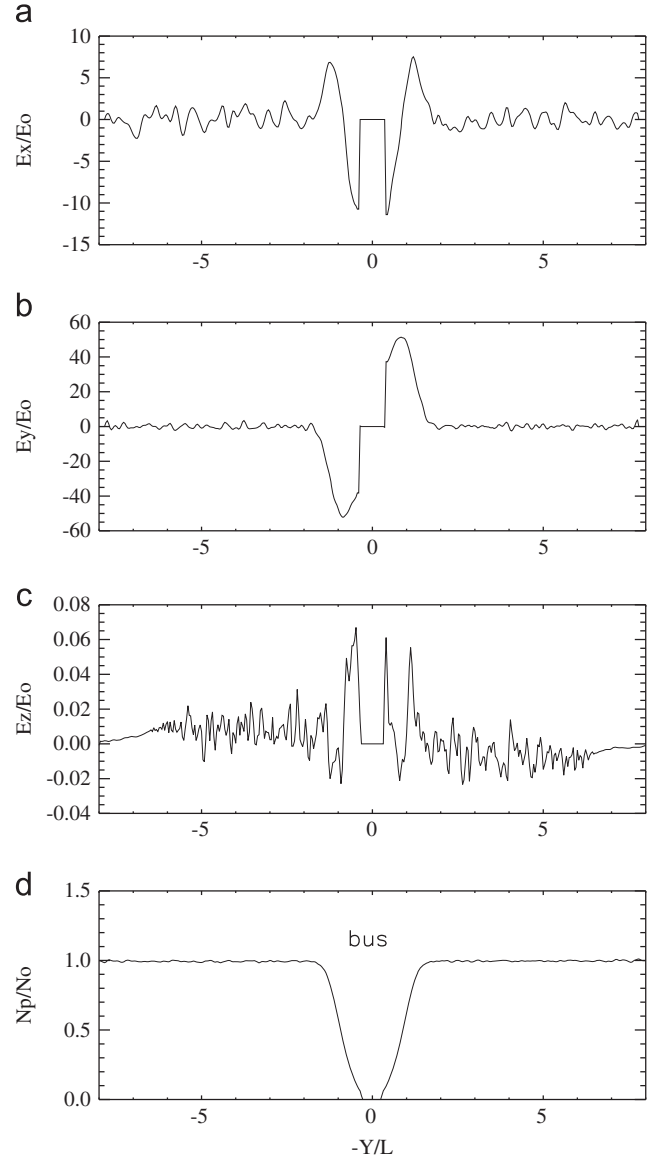


Fig. 4. The 1D cuts for the electric field components $E_x(E_0)$, $E_y(E_0)$ and $E_z(E_0)$ ($x=1.5$). Non-linear saturation of the perturbations at $t = 15 T_{ce}$.

same plasma parameters but with grid spacing two times smaller. One may see that the level of fluctuations in E_x and E_y are a little bit higher when modeling with higher spatial resolution.

Our hybrid modeling work fits very well under the assumption of quasi-neutrality. In the general case, there is also a possibility for formation of electron beams and excitation of the plasma waves ($\omega \approx \omega_{pe}$) in regions of the plasma wake having a low ion density however, the study of these effects needs a full kinetic model (e.g., 1D electrostatic modeling of the lunar wake by Bale et al., 1997; Farrell et al., 1998; Halekas et al., 2011). The formation of an electron boundary layer near the surface of the heat shield and bus are due to spacecraft charging and photoelectrons (Ergun et al., 2010) and may support better current closure created upstream and downstream in the flow near the spacecraft.

Unfortunately, 2.5D modeling is limited to the parallel interaction case. Modeling of the quasi-parallel and oblique interactions show formation of a non-physical magnetic barrier since the magnetic field lines cannot move through a cylindrical obstacle. The 2.5D hybrid modeling also did not show excitation of whistler/Alfvén waves in the upstream connected with the

Table 3

Electromagnetic field perturbation in plasma environment near SPP, $\delta E(0.3 \text{ V/m})$, $\delta B(1500 \text{ nT})$.

Case	$t(T_{ce})$	δE_x	δE_y	δE_z	δB_x	δB_y	δB_z	E_n at bus
a	15	1.0–2.0	1.0–2.0	0.1	0.02	0.02	0.005	30–60
b	15	2.0–3.0	2.0–3.0	0.1	0.02	0.02	0.005	30–60

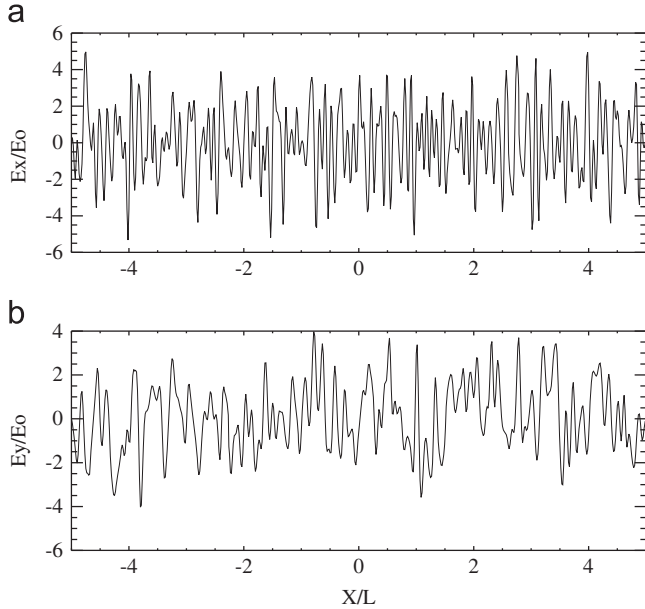


Fig. 5. The 1D cuts for the electric field components $E_x(E_0)$ and $E_y(E_0)$ ($y=0$) in absence of the spacecraft. Non-linear saturation of the perturbations at $t = 15T_{ce}$.

bi-directional current closure that was observed in the short-time 3D modeling of the SPP and near a tether in the ionosphere (Chang et al., 1994). Such a type of perturbations on a large scale (Alfvén wing) was observed near the Jovian moons, see e.g., Neubauer (1980), and plasma clouds that move across the magnetic field (Lipatov, 2002).

3.2. Perturbations in solar wind in the absence of the SPP spacecraft

In Section 3.1 we had estimated the maximum value of the electric field perturbations due to “shot” noise, Eqs. (15) and (16). We have repeated the modeling with the same parameters of the solar wind but without a spacecraft in the computational domain. Fig. 5 shows 1D cuts of the perturbation in the electric field along the x -axis ($y=0$). One may see the homogeneous perturbations with an amplitude of about $(2-4)E_0$ and a wavelength of about $(1-2)L/6 = (0.4-0.8) \text{ m}$. The profile for E_y component is more strongly modulated, Fig. 5(b), than the E_x component, Fig. 5(a). These types of short wavelength fluctuations in the electric field may present realistic perturbations in the solar wind. To find these perturbations in the electric field one needs to estimate the number of the physical particles per each grid cell and then use the local values of the Mach number, electron beta and the motional electric field E_0 , Eq. (16). For solar wind at a distance $r = R_S$ the plasma density is about $5 \times 10^3 \text{ cm}^{-3}$ and, hence, the number of the macro-particles per cell is about 625×10^3 . For these parameters, Eq. (16) gives the following values for the fluctuations of the polarization electric field, $\delta E_{pol} \approx 1 \times E_0$.

The particle motion through the short wavelength electric field oscillations results in the extra heating of the particle and, hence, in the change of the macroscopic parameters of the solar wind.

Note that these effects may be investigated in detail by the use of the particle-in-cell hybrid or full-kinetic methods because the “shot” noise is an intrinsic attribute of these methods.

4. Conclusions and possible future modeling

The 2.5D hybrid modeling is used to describe global solar wind plasma dynamics near the SPPSC at $r = 9.5R_S$, and it has demonstrated several following features:

- The 2.5D modeling shows the formation of an extended plasma wake with a small density cavern around the spacecraft. The large spatial wake results in the reduction of the polarization field near the SC and behind the spacecraft bus up to 3.0–9.0 V/m and 18 V/m, respectively, in comparison with 3D (short-time) modeling 9.0–60 V/m.
- The 2.5D modeling shows compression-like perturbations in the E field, possibly associated with “shot” noise. Unfortunately, 2.5D modeling of the parallel SW-SPP interaction does not demonstrate a two-current system upstream of the heat shield that was seen in the 3D hybrid short-time modeling for $\theta_{U_0, B_0} = 11^\circ$.
- The 2.5D modeling with a particle reflection boundary condition at the heat shield (have not been shown in this article) shows the formation of enhanced density in the external region of the plasma wake. Upstream of the SPP, the plasma velocity distribution may change a lot due to possible two-stream (beam-beam) instability.
- Electric field perturbations from modeling are comparable to or exceed the maximum electric field expected for the SPPSC. The values of the electric field oscillation near the SC’s bus may be the same order as the maximum expected electric field (d.c.) in an antenna (see Murphy et al., 2008, Table 1). Therefore, wake deployment of an electric field plasma-wave antenna may not be a viable option for scientific measurements on board the SPPSC in the inner heliosphere. The strong electromagnetic perturbation in the SW by the SC may cause the same problems with the scientific measurements on board the SC in the Solar Orbiter mission.
- The strong perturbations in the electric field due to “shot” noise may have an important effect on solar wind heating and, hence, the acceleration/deceleration of the solar wind.
- Our modeling may also be very important for study of the plasma environment near small bodies near the Sun, e.g., Vulcanoid asteroids.

Future modeling with a full particle code applied in the vicinity of the SC and is incorporated in the global hybrid code will take into account SC charging, charge separation effects, outgassing from the heat shield, photoionization and electron impact ionization effects near the SC. The photo and secondary electrons may create a boundary layer near the heat shield that may play an important role in the formation of current closure around the spacecraft. We need to perform longer time, 3D modeling in order to obtain a “steady-state” solution with the formation of a plasma wake in a quasi-parallel interaction. We also need to study non-stationary processes when the interaction of the SPP occurs with interplanetary shocks or Coronal Mass Ejection events. We are now in a position to do this, since these codes have been converted to the hybrid MPI/OpenMP environment to achieve improved scalability for longer computations.

Acknowledgments

E.C. Sittler and A.S. Lipatov were supported in part by NASA Grant no. 93672302010619 (PI—E.C. Sittler) through NASA GSFC

and GPIH/GEST Center UMBC, respectively. Computational resources were provided by the NASA's High-End Computing Center at NASA Goddard Center and Advanced Supercomputing Division at Ames Center through the NASA Computational Grants SMD-07-0458 and SMD-08-0636.

References

- Alpert, Ya.L., 1974. Waves and Satellites in the Near-Earth Plasma. Studies in Soviet Space (from Russian by J.B. Barbour, Trans.). Consultants Burea, New York, p. 205.
- Alpert, Ya.L., Gurevich, A.V., Pitaevskiy, L.P., 1965. Space Physics with Artificial Satellites (from Russian by H.H. Nickle, Trans.). Consultants Burea, New York p. 240.
- Bale, S.D., Owen, C.J., Bougret, J.I., Goetz, K., Kellogg, P.J., Lin, R.P., Manning, R., Monson, S.J., 1997. Evidence of currents and unstable particle distributions in an extended region around the lunar wake. *Geophysical Research Letters* 24, 1427–1430.
- Birdsall, C.K., Langdon, A.B., Okuda, H., 1970. Finite-size particle physics applied to plasma simulation. In: Alder, B., Fernbach, S., Rotenberg, M. (Eds.), *Methods in Computational Physics. Plasma Physics*, vol. 9. , Academic Press, New York and London, pp. 241.
- Braginskii, S.L., 1965. Transport processes in a plasma. In: Leontovich, M.A. (Ed.), *Reviews of Plasma Physics*. , Consultants Burea, New York, pp. 205.
- Chang, C.L., Lipatov, A.S., Drobot, A.T., Papadopoulos, K., Satya-Narayana, P., 1994. Hybrid simulation of whistler waves generation and current closure by a tether in the ionosphere. *Geophysical Research Letters* 21, 1015.
- Ergun, R.E., Malaspina, D.M., Bale, S.D., McFadden, J.P., Larson, D.E., Mozer, F.S., Meyer-Vernet, N., Maksimovic, M., Kellogg, P.J., Wygant, J.R., 2010. Spacecraft charging and ion wake formation in the near-Sun environment. *Physics of Plasmas* 17 (072903), 1–9.
- Farrell, W.M., Kaiser, M.L., Steinberg, J.T., Bale, S.D., 1998. A simple simulation of a plasma void: applications to wind observations of the lunar wake. *Journal of Geophysical Research* 103 (10), 23653–23660.
- Halekas, J.S., Saito, Y., Delory, G.T., Farrell, W.M., 2011. New views of the lunar plasma environment. *Planetary and Space Science* 59 (13), 1681–1694.
- Lipatov, A.S., 1976. About the three-dimensional structure of the lunar wake. *Cosmic Research* 14, 103.
- Lipatov, A.S., 2002. The Hybrid Multiscale Simulation Technology. An Introduction with Application to Astrophysical and Laboratory Plasmas. Springer-Verlag, Berlin, Heidelberg, New York.
- Lipatov, A.S., Motschmann, U., Bagdonat, T., Griesmeier, J.-M., 2005. The interaction of the stellar wind with an extrasolar planet—3D hybrid and drift-kinetic simulations. *Planetary and Space Science* 53, 423–432.
- Mankofsky, A., Sudan, R.N., Denavit, J., 1987. Hybrid simulation of ion beams in background plasma. *Journal of Computational Physics* 70, 89–116.
- Murphy, N., et al., 2008. Thermal Design Consideration for the Solar Probe Electric Field Antenna.
- Neugebauer, M., 1960. Question of the existence of a lunar magnetic field. *Physical Review Letters* 4 (1), 6–8.
- Neubauer, F.M., 1980. Nonlinear standing Alfvén wave current system at Io—Theory. *Journal of Geophysical Research* 85, 1171–1178.
- Olson, J., Miloch, W.J., Ratynskaia, S., Yaroshenko, V., 2010. Potential structure around the Cassini spacecraft near the orbit of Enceladus. *Physics of Plasmas* 17, 102904.
- Wang, Y.C., 1968. Theoretical study of the magnetic field in the lunar wake. *Physics of Fluids* 11 (8), 1713.
- Wang, Y.C., 1969. Field and plasma in the lunar wake. *Physical Review* 186 (1), 143.
- Wang, Y.C., Ness, N.F., 1970. Observations and interpretation of the lunar Mach cone. *Journal of Geophysical Research* 75 (31), 6002–6010.